PERGAMON

Aerosol Science 34 (2003) 383–403

Journal of
Aerosol Science

www.elsevier.com/locate/jaerosci

Evolution of structure and charge of soot aggregates during and after formation in a propane/air diffusion flame

A.A. Onischuk[a,*], S. di Stasio[b], V.V. Karasev[a], A.M. Baklanov[a], G.A. Makhov[a], A.L. Vlasenko[a], A.R. Sadykova[c], A.V. Shipovalov[c], V.N. Panfilov[a]

[a] *Institute of Chemical Kinetics and Combustion, Siberian Branch of the Russian Academy of Sciences, 630090 Novosibirsk, Russia*

[b] *Istituto Motori C.N.R., Fluid Dynamics and Combustion Division, Via Marconi 8, 80125 Napoli, Italy*

[c] *Novosibirsk State Pedagogic University, Novosibirsk, Russia*

Received 4 April 2002; accepted 11 December 2002

Abstract

Evolution of soot aggregate morphology, size and concentration is investigated during and after formation of soot in propane/air diffusion flame. Monitoring of gaseous intermediates in the flame is done by gas chromatography. Soot aggregate size and morphology are analyzed by a transmission electron microscope; soot number concentration is determined by an automated diffusion battery. Aggregate–aggregate collisions and aggregate structural transformations are observed in real time using a video system. It is determined that soot aggregates formed in flame are charged. The electric charge per aggregate is determined by video observation of aggregate movement in electric field. Both positively and negatively charged aggregates are formed. Typical net charge per aggregate is a few elementary units. An effect of soot aggregate restructuring from chain-like to compact structures is observed. It is determined that the driving force for this restructuring is Coulomb interactions between different parts of the aggregate. It is demonstrated that Coulomb interactions between aggregates can affect considerably coagulation process and the final aggregate shape.

Keywords: Soot; Aggregate; Charge; Coagulation; Restructuring; Fractal dimension

1. Introduction

Soot is usually a byproduct of incomplete hydrocarbon combustion generated in regions of the flame where not enough oxygen is present to yield a complete conversion of fuel into carbon dioxide

* Corresponding author. Fax: +7-3832-352350.
E-mail address: onischuk@ns.kinetics.nsc.ru (A.A. Onischuk).

0021-8502/03/$ - see front matter
doi:10.1016/S0021-8502(02)00215-X

and water. The earliest stage of soot generation is believed to be the formation of 5–10 nm particles due to reactive coagulation of polycyclic aromatic hydrocarbon (PAH) molecules (Appel, Bockhorn, & Frenklach, 2000; Frenklach & Wang, 1994). These particles are more transparent to a transmission electron microscope (TEM) electron beam than the more mature soot particles and are often referred as soot precursor particles (Köylü, Mcenally, Rosner, & Pfefferle, 1997; di Stasio, 2001a; Dobbins & Subramaniasivan, 1994; Vander Wal, 1996). The later stages are characterized by simultaneous coagulation, coalescence and surface growth of precursors leading to an increase of the particle size. Simultaneously an internal rearrangement of the precursor particles occurs resulting in structures with more condensed aromatic rings and more compact shape called "soot nuclei" (D'Anna, D'Alessio, & Minutolo, 1994). These nuclei grow due to coagulation and surface reactions, forming the final aggregates.

The soot aggregate morphology is of great importance from the environmental point of view. In particular, practical combustion systems generally produce measurable amounts of PAHs which are associated with adverse neurotoxic, cancerogen and mutagen effects in humans. Much of the current interest in control of soot emission is based on the observation that mutagen compounds can be adsorbed onto particle surfaces (Koshland, 1996; Longwell, 1982). The morphology of soot aggregates is an important factor which determines the transport characteristics of soot in the atmosphere and penetration in the human lungs. It was supposed that Coulomb interactions may play a considerable role in the aggregation process and affect essentially the aggregate morphology (Richter, Sander, & Cheng, 1984; Hurd & Flower, 1988; Zhang, Sorensen, Ramer, Olivier, & Merklin, 1988; Julien & Meakin, 1989; Onischuk et al., 2000). It was shown (Place & Weinberg, 1966; Ball & Howard, 1971; Wersborg, Howard, & Williams, 1973) that soot aggregates formed in flame are charged. However, there is no detailed contributions in the literature which give correlation of soot aggregate morphology with soot formation conditions.

The objectives of this paper are to study the evolution of soot aggregate morphology, size and concentration in comparison with concentrations of gaseous intermediates in a diffusion flame of propane; to carry out the aggregate shape and size monitoring after flame; and to demonstrate that Coulomb interactions play an important role in soot aggregate coagulation and restructuring.

2. Experimental

The experimental setup is given in Fig. 1. Soot was formed in a propane/air diffusion flame. A cylindrical burner with an inner diameter of 1 cm was fed with pure propane (99.8%) at 4 cm^3/s (at atmospheric pressure and room temperature). The length of the visible part of the flame was 12–14 cm. To avoid the influence of air fluctuations the flame was shielded by a co-annular cylindrical iron grid of diameter 7 cm. Gas chromatography was used to determine the propane conversion and gaseous intermediate concentrations. Gaseous samples for analysis were sucked from the flame axis through a 0.8 mm stainless steel capillary pipe at different heights above burner. Identification of species was accomplished by matching the gas-chromatographic retention times to pure components.

TEM analysis of soot was carried out using JEM-100SX electron microscope. To investigate soot evolution in the flame we used a thermophoretic technique which seems to be the most appropriate for soot sampling from a flame (Köylü et al., 1997; Dobbins & Subramaniasivan, 1994). The sampling procedure was as follows. The electron microscopy grid (covered with a thin polyvinylformval film)

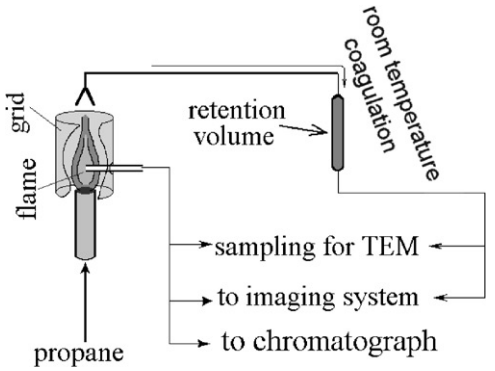

Fig. 1. Schematic diagram of the experimental setup.

was attached to a special metal support (the width of the support was 0.5 cm, the thickness was 0.02 cm). This support inserted the grid with a high speed to the axis of the flame. The residence time was determined by CCD camera observation. The residence time at the axis was varied in the range 0.1–0.5 s. The time of flight of the support through the peripheral zone of the flame was an order of magnitude less than the residence time.

Soot aggregate evolution at room temperature was also investigated by TEM. Soot was sucked at a rate of 7 cm^3/s from the overflame region ($h = 30$ cm) to an aerosol duct of a the gas temperature close to room temperature. We investigated size and morphology of soot aggregates sampled after coagulation time in the range 1–1000 s. This room temperature coagulation time was regulated by retention bulbs. The sampling of soot from the flow was carried out by a thermal precipitator.

The soot mass concentration in the flame was determined by sampling aerosol from the axis of the flame through a copper tube (i.d. = 3 mm, length = 5 cm) at 0.5 cm^3/s at STP onto a filter. The mass of deposit on the filter was determined by weighing.

Number concentration and size of soot particles at low heights above burner were determined using an automated diffusion battery (ADB) coupled with a condensation chamber and a condensation nucleus counter (Ankilov, Baklanov, Mavliev, & Eremenko, 1991). To this end, the aerosol was sampled from the flame axis through the same copper tube described above and then diluted 400 times at the exit of the tube by the filtered air. Downstream, the flow was diluted again in two dilution cascades to a concentration of 10^4 cm^{-3}. The ADB setup was used when the particle number concentration in the flame was less than 10^9 cm^{-3}. Measurements at larger concentrations were not possible because of coagulation in the sampling tube.

Coagulation was also observed in real time using an imaging system. To this aim, a small portion of aerosol was sucked from the flow outgoing from the retention bulbs and injected to an optical cell described by Fuchs and Petrianov (1933). Light scattered from a He–Ne laser beam at an angle of 90° passed through a flat window to a microscope objective and then to a CCD camera connected to a TV system. The objective forms an image at the light sensitive matrix with the magnification of 15 times. The visualization field in the optical cell is about 300×400 μm^2. The focal depth in the object space is $\sim$30 μm, the spatial resolution of the system is 3 μm. This optical setup resolves images of aggregates larger than about 3 μm; smaller aggregates were visible as spots. To create an electric field, two parallel electrodes were fixed in the cell at a distance of 0.25 cm. The movement

of the aggregates in the electric field gave information on the electric charge and dipole moment of aggregates.

3. Results and discussion

3.1. Monitoring of chemical gaseous species and solid particles within the flame

The axial and radial flame temperature profiles were measured by a chromel–alumel thermocouple with a junction size of 200 μm. The flame temperature measurements were corrected for radiation losses (Kaskan, 1956). For example, at flame temperature 1700 K the correction was 50 K. To be sure that the heat removal through the wires do not disturb the measurement results we used both usual 100 μm wires and the wires with a larger diameter of 500 μm. In both cases the results were the same within the experimental accuracy. Fig. 2a shows the axial temperature profile. One can see that the region between 0 and 2 cm above burner is characterized by a sharp temperature increase. At $h = 2$ cm the temperature is about 1200 K. Above this, temperature increases more slowly with h at a rate of approximately 30 K/cm. Fig. 3 shows radial temperature profiles for $h=0.5$ and 1.8 cm.

Fig. 4 shows an example of the gas chromatogram of the mixture sampled from the flame axis at $h = 3.2$ cm. Figs. 2b–d show the concentrations of propane and gaseous intermediates at the flame axis as a function of h. As examples we show the concentrations of C_2H_2, benzene and toluene. These species are of interest because benzene and toluene are minor representatives of PAHs, while acetylene and PAHs play an important role in soot formation. In particular, acetylene is a construction material for PAHs, and the nucleation process is believed to be controlled by the reactive coagulation of PAH molecules (Appel et al., 2000; Frenklach & Wang, 1994; Macadam, Beer, Sarofim, & Hoffmann, 1996). Besides, both PAHs and acetylene are important soot surface growth agents (Macadam et al., 1996). Figs. 2c and d show a simultaneous increase of C_2H_2 and aromatic species concentrations in the range of $0 < h < 1$ cm. This simultaneous increase is in agreement with the accepted point of view that acetylene is a construction material for aromatic molecules (Frenklach & Wang, 1994; Appel et al., 2000; Nemeth & Heberger, 1998).

Fig. 2e shows the soot mass concentration in the flame as a function of height above burner. This concentration was determined from the soot mass concentration measured at room temperature in the samples drawn from the flame axis. To estimate the soot concentration in the flame we divided the room temperature concentration values by the gas thermal expansion factor equal to the ratio between the flame temperature and room temperature (Fig. 2a). From Fig. 2 one can see that soot particle formation starts at $h \approx 1$ cm when the propane conversion is about 60%, on the other hand, the rate of aromatic species accumulation decreases at the same $h \approx 1$ cm. This correlation between the soot inception and aromatic species accumulation is in agreement with the modern point of view that the soot nucleation process is controlled by the reactive coagulation of large PAH (Appel et al., 2000; Frenklach & Wang, 1994; Macadam et al., 1996; Nemeth & Heberger, 1998). One can also see that in the region $1 < h < 4.5$ cm the aromatic species concentration increases again. This increase can be attributed to the decrease in aerosol particle reactivity during the growth process (Macadam et al., 1996) resulting in the decrease of PAH consumption in the reactions of soot particle surface growth. At $h > 5$ cm one can see a simultaneous decrease of C_2H_2 and aromatic species concentrations

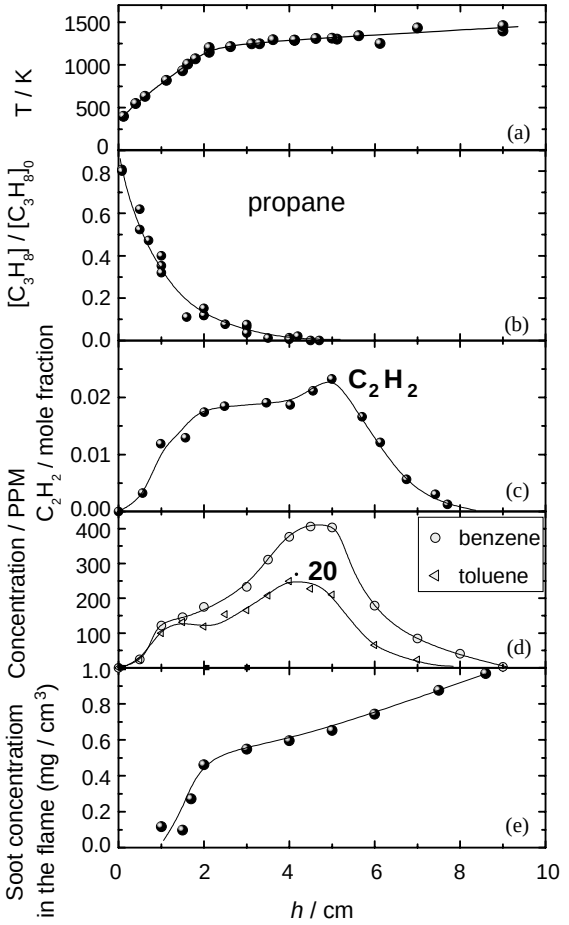

Fig. 2. (a) Axial temperature profile in the flame. (b)–(d) Gaseous concentrations of propane and intermediates in the mixtures sampled from the axial positions of the flame. $[C_3H_8]$ and $[C_3H_8]_0$ are propane concentrations in the sampled mixture and in the initial fuel gas fed to the burner, respectively. (e) Soot mass concentration at the flame axis vs. height above burner. (h) is height above burner. Lines are smooth fit through data.

(Figs. 2c and d) with h. This decrease is evidently caused by the depletion of propane by this height (Fig. 2b).

The soot mass concentration increases very rapidly in the range $1 < h < 2$ cm and then more slowly (Fig. 2e). The rate of increase of C_2H_2 concentration also decreases at $h \approx 2$ cm. This behavior of soot and C_2H_2 concentrations correlates with the axial temperature profile (Fig. 2), probably due to the temperature dependence of pyrolysis rate.

Fig. 5 shows TEM micrographs of soot aggregates sampled at different heights above burner. Soot particles in the range $2 \leqslant h \leqslant 4$ cm were mostly observed as single "precursor particles" or "elementary particles", which are relatively translucent under the electron beam. The majority of these single particles has no definite border. At $h > 4$ cm soot aerosol consists mostly of aggregates composed of primary particles. At $h < 10$ cm the primary particles seem to become fused, evidently

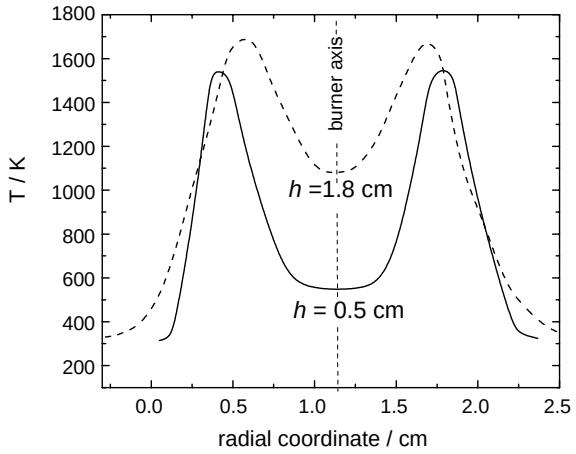

Fig. 3. Radial temperature profile at height above burner $h = 0.5$ and 1.8 cm.

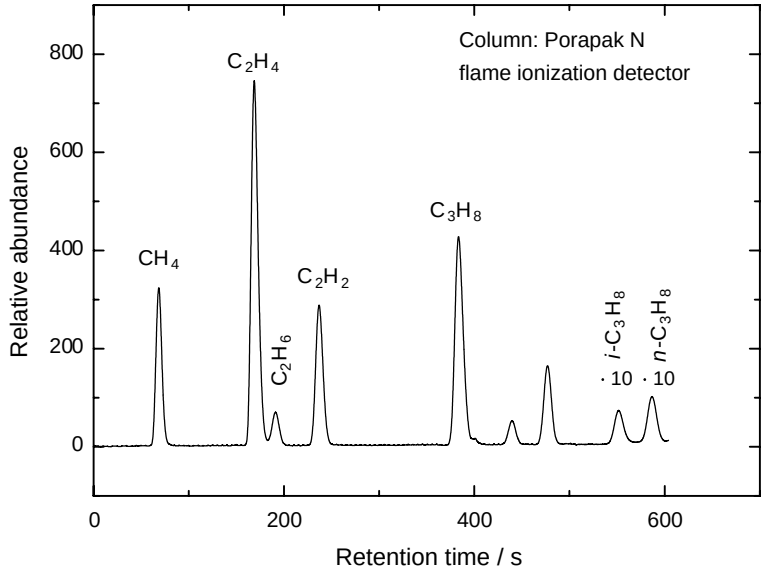

Fig. 4. Gas chromatogram of the mixture sampled at height above burner $h = 3.2$ cm from the axial position of the flame.

due to the high rate of surface growth by PAH and acetylene addition. Fig. 5d shows soot aggregates collected at $h = 11$ cm. The primary particles in these aggregates are seen clearly due to the fact that both propane and gaseous intermediates are depleted by this height above burner (Figs. 2b–d). Thus, the aggregation process is mainly governed by the coagulation process at this stage. One can see that the size of primary particles decreases with h increasing in the range $7 < h < 11$ cm. This decrease of the primary particle size is related to the oxidation of soot particles (Köylü et al., 1997; Megaridis & Dobbins, 1989), and/or carbonization (Reilly, Gieray, Whitten, & Ramsey, 2000).

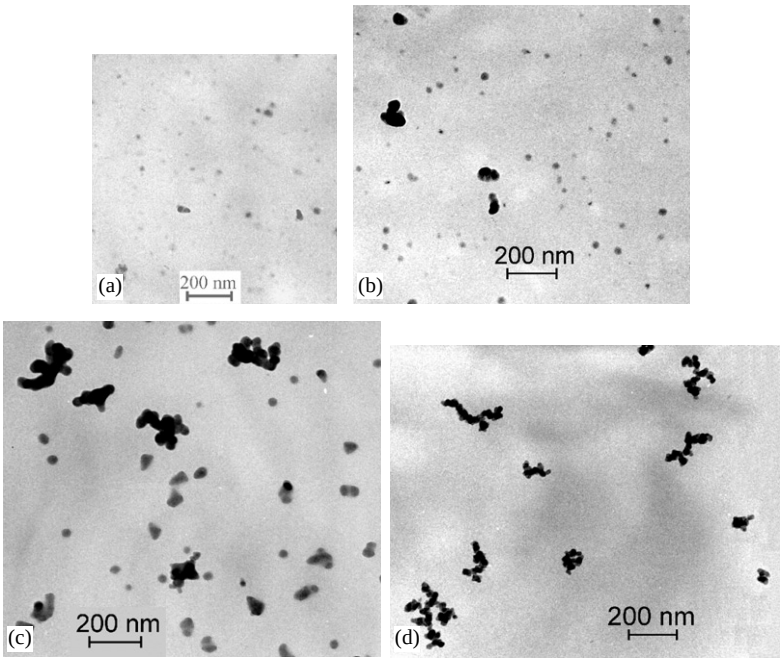

Fig. 5. TEM micrographs of soot particles sampled from the flame axis at $h = 2$ (a), 4 (b), 7 (c), 11 cm (d).

Using the TEM images the average radius of aggregates and/or precursor particles was measured as a function of the height above burner. The radius was determined as

$$R = \tfrac{1}{2}\sqrt{LW}, \tag{1}$$

where L and W are the dimensions of the rectangle enclosing the image of single particles or aggregate (Rogak, Baltensperger, & Flagan, 1991). Fig. 6 shows the average radius R determined from the TEM data (solid symbols). We have also inserted the data determined by the ADB (open symbols). One can see that there is a reasonable agreement between geometric and mobility equivalent diameters.

Fig. 7 presents soot particle number concentration vs. height above burner. Open points were determined by the ADB, solid triangles are points estimated from the mass concentration data (Fig. 2e) and mean aggregate mass determined from TEM micrographs. To estimate the mass per aggregate we need the aggregate volume. To this end, each aggregate was subdivided to subunits. These subunits were approximated by spheres, cylinders or ellipsoids of revolution. Most often the size of these subunits was equal to size of primary particles. Sometimes a group of closely packed primary particles was considered as a subunit. As a rule the overlapping subunits were sufficiently distinguished in the micrographs. Therefore, we suppose that this method of estimation of the agglomerate volume gives a satisfactory information in spite of the fact that we use 2D projections. When estimating the aggregate mass the density of the material was taken as $\rho \approx 2$ g/cm^3 (which is a value typically used in such kind estimations, see, for example, Benish, Lafeur, Taghizadeh, & Howard, 1996; Knorre, Tanke, Thienel, & Wagner, 1996).

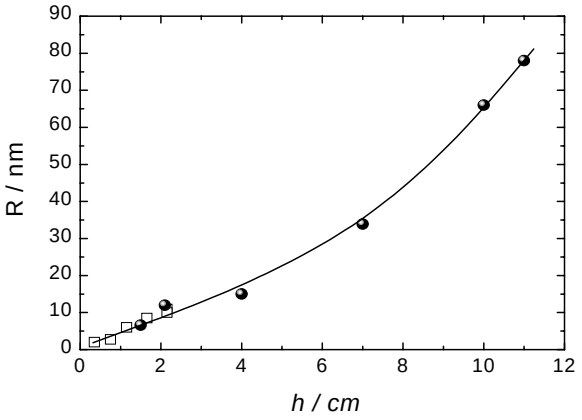

Fig. 6. Mean arithmetic radius of aggregates vs. height above burner. (□) data determined by the ADB; (●) TEM data. Line indicates trend.

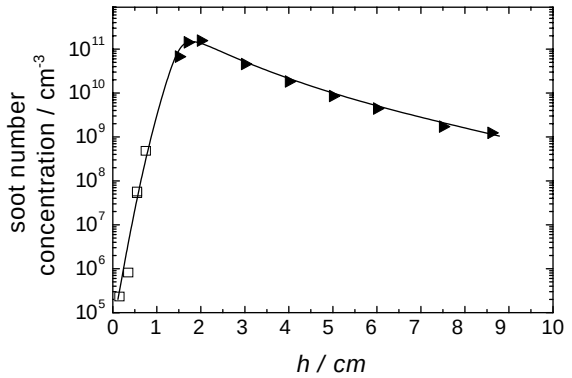

Fig. 7. Soot particle number concentration vs. height above burner. (□) data determined by the ADB; (▲) the number concentration points estimated from the mass concentration data (Fig. 2e) and mean aggregate mass determined from TEM micrograms. Line is smooth fit through data.

The aggregate distribution vs. radius R is well described by a lognormal function with the mean geometric standard deviation $\sigma_g \approx 1.8$ (Fig. 8).

We described the aggregate morphology in terms of fractal-like dimension D_f which can be determined from a power relation between the mass M of each aggregate and its radius R measured by TEM analysis (Rogak et al., 1991; Rogak, Flagan, & Nguyen, 1993; Katzer, Weber, & Kasper, 2001a, b; Forrest & Witten Jr., 1979; Schmidt-Ott, 1988; Weber, Baltensperger, Gäggeler, & Schmidt-Ott, 1996; Zhang et al., 1988; Samson, Mulholland, & Gentry, 1987; Martin, Schaefer, & Hurd, 1986; Wiltzius, 1987; Jang & Friedlander, 1998):

$$M \propto R^{D_f}. \tag{2}$$

To determine D_f the values of aggregate masses were plotted as $\log M$ vs. $\log R$. When determining D_f at $h \leqslant 4$ cm only aggregates were taken into consideration, single particles were omitted.

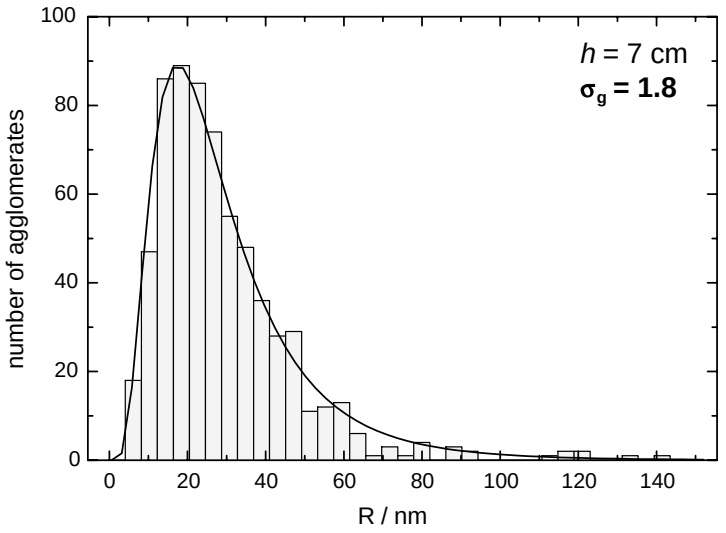

Fig. 8. Frequency distribution of agglomerate radius R determined from TEM measurements; the height above burner $h = 4$ cm. Solid line is a lognormal function with mean geometric standard deviation $\sigma_g = 1.8$.

We found that the fractal dimension D_f depends on h. At $h = 2$ cm the fractal dimension is about 2.5 and at $h = 11$ cm, $D_f = 1.7$. The reason for the large values of the fractal dimension at low h lies probably in a high contribution of the surface reactions of acetylene addition via HACA mechanism (Appel et al., 2000; Frenklach & Wang, 1994; Mauss, Trilken, Breitbachh, & Peters, 1994; Bochhorn & Schäfer, 1994) and PAH addition (Macadam et al., 1996; Marquardt, Mauß, Jungfleisch, Suntz, & Bockhorn, 1996) to the growth of soot aggregates. TEM images support this suggestion (see, for example, Figs. 5a–c). The low fractal dimension $D_f = 1.7$ at $h = 11$ cm is explained by the fact that the gaseous intermediates are depleted at high h (see Fig. 2). Therefore, the soot growth is governed by diffusion-limited cluster–cluster aggregation mechanism (Forrest & Witten Jr., 1979; Schmidt-Ott, 1988; Weber et al., 1996; Zhang et al., 1988; Samson et al., 1987; Martin et al., 1986; Wiltzius, 1987; Jang & Friedlander, 1998) at this stage (compare with $D_f = 1.7$ for the aggregates sampled from the afterflame region (Section 3.3) for the coagulation time $t < 200$ s).

3.2. The role of the electric charge in the aggregation process

We observed the movement of soot aggregates in the homogeneous electric field (160 V/cm) using the imaging system. The aggregates were sampled from the axis of the flame at different heights above burner. The experiment was carried out as follows. The gas with aggregates was sucked through a capillary to the optical cell. The flow rate through the capillary was 0.5 cm^3/s (at room temperature). The time of passing through the tubes from the flame to the optical cell is 30 s. During this passage the coagulation occurred which can affect the frequency distribution of the aggregate charge. Nevertheless, the video observations of these final aggregates gave some idea about the possible electric charge of soot aggregates in the flame.

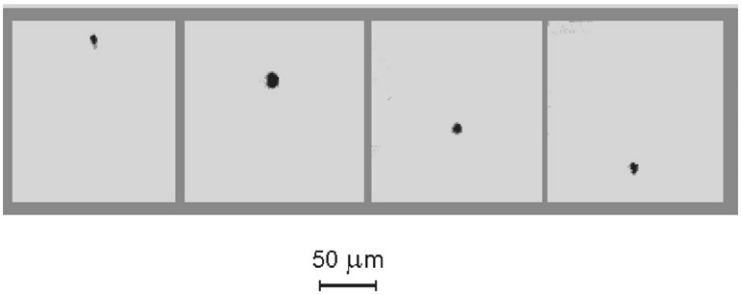

Fig. 9. A series of frames demonstrating movement of a charged soot aggregate in the electric field. The frames are separated by a time interval of 0.08 s. The field is oriented vertically. The sample was sucked to the video system from the flame axis at height above burner $h = 4$ cm.

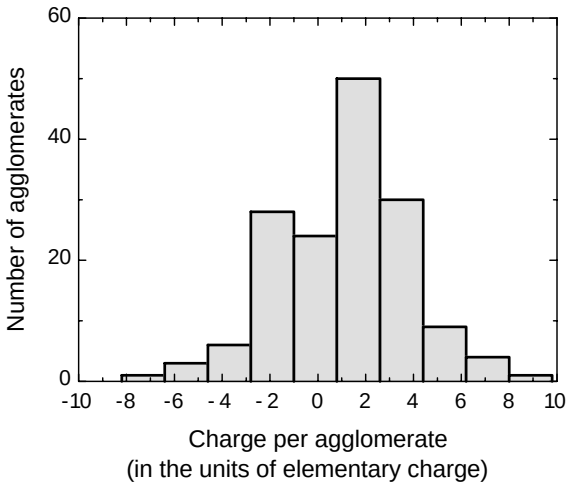

Fig. 10. Frequency distribution of agglomerate charge. Soot aggregates were sucked from the flame axis at $h = 5$ cm. Mean arithmetic radius of aggregates in the optical cell is $R = 400$ nm.

The observations showed that the majority of aggregates was charged, i.e. aggregates drifted along the field or against the field. Fig. 9 shows a negatively charged aggregate moving in the electric field. It is possible to estimate the velocity of aggregate movement from these frames. The aggregate charge was estimated from the balance between the friction force and the Coulomb force assuming equivalence of the mean mobility radius R_m and mean projected area radius R_a (Rogak et al., 1993). The arithmetic mean R_a was determined by TEM for the conditions mentioned above. Fig. 10 shows the frequency distribution of soot aggregate charge at $h = 5$ cm. One can see from the figure that most often the aggregate charge is about a few elementary units. We found that about 20% of aggregates were neutral, 50% were positively charged and 30% were negatively charged. This ratio between the negative, positive and neutral aggregates does not depend on the height above burner in the range 1.5–5 cm. Approximately the same ratios between positive and negative soot particles were measured by Roth and Hospital (1994) for premixed flat flames of acetylene and oxygen. The

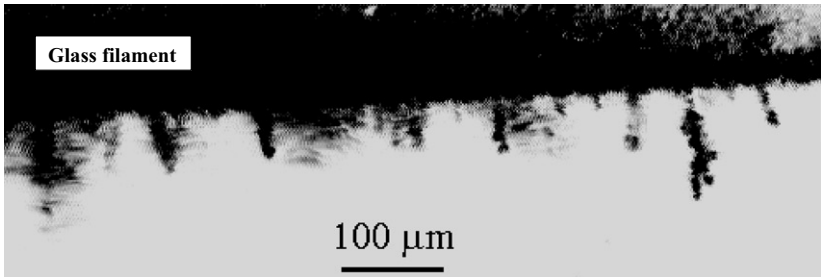

Fig. 11. Dendrites on the surface of glass filament formed after the injection of soot aerosol into the optical cell.

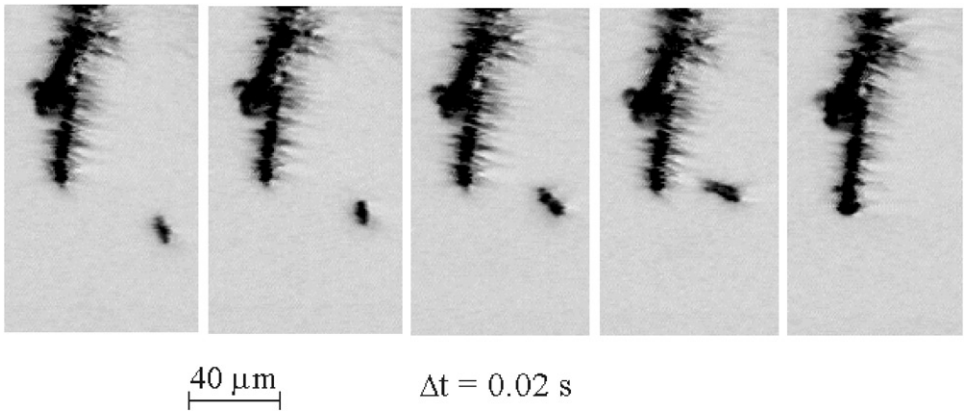

Fig. 12. Imaging system results illustrating soot agglomerate–tendril collisions. The picture is represented by a series of frames separated by a time interval of $\Delta t = 0.02$ s. Time increases from left to right.

reason for the aggregates to be charged is ion formation in the flame. The accepted prime source of ion formation in sooting flames is the chemiionization reaction (Calcote & Gill, 1994)

$$CH + O \rightarrow HCO^+ + e^-. \quad (3)$$

To understand how significant is the role of Coulomb interactions in the soot coagulation process we observed the sticking of free aggregates to a thin glass filament (diameter 0.03 cm) fixed inside the imaging system optical cell. The microscope objective was focused at the surface of this filament. Then the soot aerosol sampled at $h = 30$ cm was injected to the optical cell. Soon after the aerosol injection we observed formation of dendrites on the surface of this filament. Then the free aggregate sticking to the dendrites was observed. Fig. 11 shows the dendrites on the surface of the filament. The sticking process is illustrated in Fig. 12 by a sequence of frames recorded of a time interval of 0.02 s. Fig. 13 represents the time plot of the distance observed between the dendrite and the aggregate shown in Fig. 12. It is evident from the figure that the aggregate velocity increases progressively with time, caused by some sort of attractive interaction between the aggregate and the dendrite.

Using the imaging system we also observed aggregate–aggregate collisions. The experiment was carried out as follows. The aerosol sample obtained at $h = 30$ cm was injected to the optical volume.

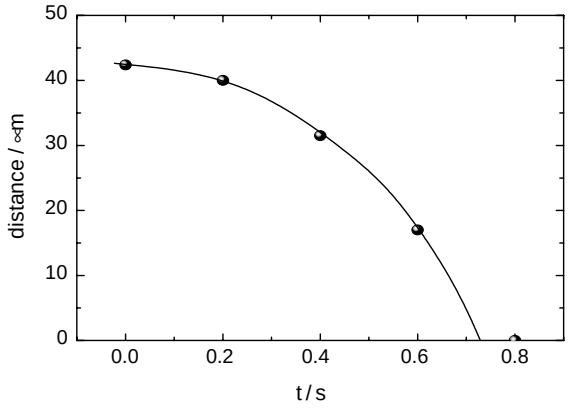

Fig. 13. The distance between the soot aggregate and the dendrite (presented in Fig. 12) vs. time. Line indicates trend.

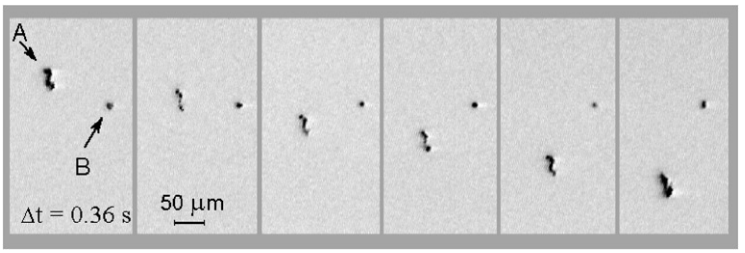

Fig. 14. Sequence of frames illustrating the movement of two aggregates "A" and "B" in a homogeneous electric field of 160 V/cm. The field is oriented vertically. The time interval between the frames is $\Delta t = 0.36$ s. Time increases from left to right.

After the injection the coagulation continued in the optical cell (without electric field). Soon large enough aggregates with the size of a few micrometers were observed. We chose two aggregates and looked after them. First, we applied an electric field and observed a movement of the aggregates under consideration in this electric field. This movement gave information on the net charge of each aggregate considered. Besides, we observed rotations of aggregates when switching the polarity of the electric field. These rotations gave an information on the aggregate dipole moments. Then the electric field was switched off and we observed the relative movement of aggregates without any external influences. Fig. 14 shows two aggregates in an electric field of 160 V/cm denoted by letters "A" and "B". One can see that the aggregate "A" moves downwards. This movement means that this aggregate is positively charged. The aggregate "B" does not move in the field. This means that the net charge of the aggregate "B" is equal to zero. Analyzing the image of the aggregate "A" at low illumination we determined that the length L of this aggregate is about 20 μm. To determine the projected area radius R_a for the aggregate "A" we analyzed TEM images of 200 other aggregates. Thus, we determined that on average the aggregate length $L = 20$ μm corresponds to $R_a \approx 3.5$ μm. Therefore, we used the value of the mobility radius $R_m = 3.5$ μm for the aggregate "A" to estimate its net charge $n \approx 40$ e.u.

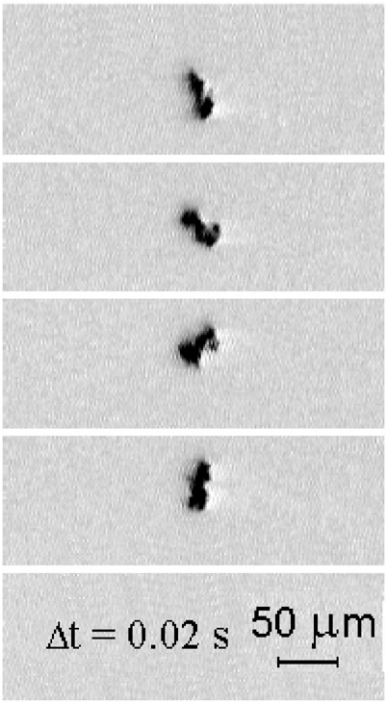

Fig. 15. Sequence of frames illustrating the rotation of the aggregate "A" (Fig. 14) when the field polarity was changed The time interval between the frames is $\Delta t = 0.02$ s. Time increases from top to bottom.

Fig. 15 shows the rotation of the aggregate "A" when the field polarity is switched. This rotation is represented by a sequence of four frames separated by a time interval of 0.02 s. This rotation testifies that the ends of this aggregate are charged oppositely. From the rotation velocity we can estimate the moment of force acting on the aggregate "A" at the time when the field polarity was changed. The aggregate rotation is governed by the equation (Fuchs, 1964)

$$\mathrm{d}\theta/\mathrm{d}\theta = B_\omega M_\theta, \tag{4}$$

where θ is the rotation angle, B_ω is the "rotation mobility", M_θ is the moment of the external force. To estimate the rotation mobility we approximate the aggregate "A" by an ellipsoid of revolution with the ratio of the major axis length to the minor axis length equal to 6. In this case we have (Fuchs, 1964)

$$B_\omega = 5.9(\pi\eta L^3)^{-1}. \tag{5}$$

Thus, from the values of $\mathrm{d}\theta/\mathrm{d}t \sim 50$ 1/s (see Fig. 15) we can estimate the moment of force M_θ using Eqs. (4) and (5) which is equal to $M_\theta \sim 3 \times 10^{-11}$ dyn cm. To have a rough idea about the possible charge distribution in this aggregate we assume that positive (q_1) and negative (q_2) charges are localized at the opposite ends of the aggregate. In this case the difference $q_1 - q_2$ is equal to the net charge $n = 40$ e.u. (see above). Finally, from (4) and (5) we have $q_1 \approx 60$ and $q_2 \approx -20$ e.u.

Fig. 16 shows the aggregates "A" and "B" when the electric field was switched off. These two aggregates stick to each other. During the sticking process the aggregate "A" changes the orientation

Fig. 16. Sequence of frames illustrating the mutual approach of the agglomerates "A" and "B" (Fig. 14) when the field was switched off. The time interval between the frames is $\Delta t = 0.02$ s. Time increases from top to bottom.

relative to the aggregate "B". Besides, these aggregates approach each other with acceleration. One can see this acceleration from Fig. 17 where the distance between the aggregates vs. time is represented. The acceleration of the mutual approach leads to the conclusion that there is some long-range interaction between the aggregates. As shown above the aggregate "A" has the net charge equal to 40 elementary units (e.u.). Meanwhile the net charge of the aggregate "B" is equal to zero. Thus, we suppose that the aggregate "B" is a dipole. We made a rough estimation of the dipole moment P_B of the aggregate "B". To this end we assumed that charges $+q$ and $-q$ are localized at the opposite ends of the aggregate. The length of this aggregate was assumed to be equal to 10 μm. We estimated the charge $q \approx 4$ e.u. from the balance between the dipole force and the drag force

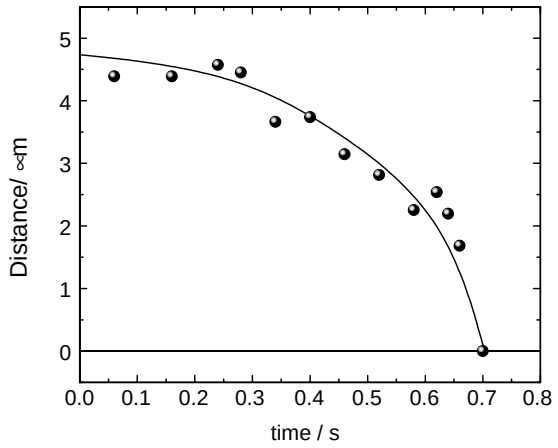

Fig. 17. Distance between the agglomerates "A" and "B" represented in Fig. 16 vs. time. Line is smooth fit through data.

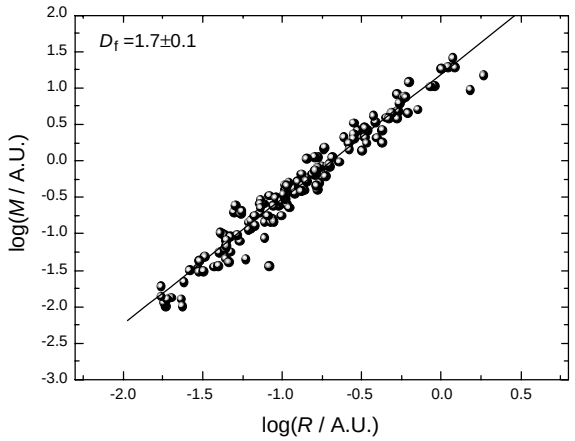

Fig. 18. $\log M$–$\log R$ dependence for room temperature coagulation time of 15 s. Solid line corresponds to the power law $M \sim R^{1.7}$.

derived from the velocity of mutual approach (Fig. 17). This charge corresponds to a dipole moment $P_B \approx 2 \times 10^{-12}$ (units CGCE).

3.3. The history of aggregate morphology at room temperature

We carried out an investigation of the aggregate evolution by collisions at room temperature, i.e. after the flame using the aerosol of $h = 30$ cm. We determined aggregate radius and fractal dimension from TEM images. Fig. 18 gives an example of $\log M$ vs. $\log R$ dependence for coagulation time $t = 15$ s.

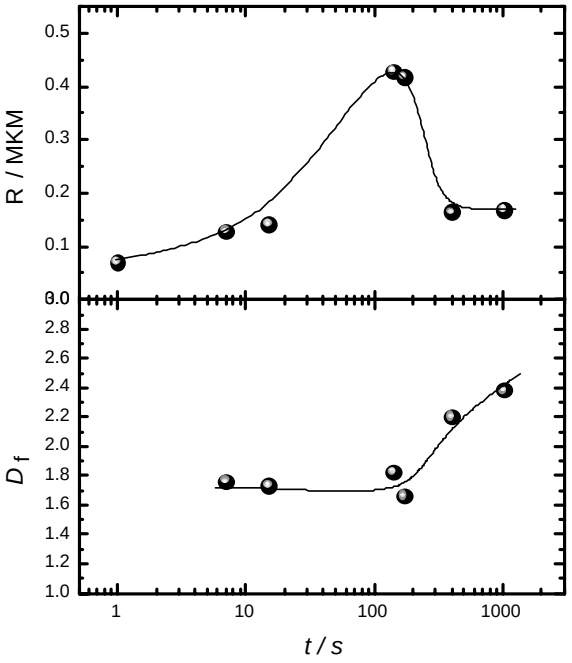

Fig. 19. Mean arithmetic radius of soot agglomerates (upper picture) and fractal dimension (lower picture) vs. room temperature coagulation time. Lines are smooth fits through data.

Fig. 19 shows the arithmetic mean aggregate radius and the fractal dimension vs. coagulation time. One can see that at the initial stage of coagulation process the aggregate radius increases monotonically with the coagulation time. The fractal dimension is approximately constant, $D_f \approx 1.7$, at this stage. After about 200 s the aggregate radius decreases with increasing time, simultaneously the fractal dimension increases from 1.7 to about 2.4 during the time interval 200–1000 s. One can assume that some aggregate restructuring occurs after 200 s. Indeed the TEM images support this assumption. Fig. 20 shows that at the initial stages of coagulation the aggregates are mostly chain-like and at the advanced stages the aggregates are mostly compact ones. We conclude that chain-like aggregates transform to compact aggregates. We directly observed this transformation process using the imaging system.

Fig. 21 shows consecutive stages of the collision of two aggregates ("A" and "B", see Fig. 21a) and a transformation of the newly formed aggregate. The experiment was carried out as follows. First, we observed the movement of these two aggregates in a homogeneous electric field (160 V/cm). We found that these aggregates were drifting in this field in opposite direction which means that these aggregates are oppositely charged. From the velocity of movement we estimated the net charges of these aggregates as -20 and $+40$ e.u., respectively. A change of the electric field polarity resulted in rotation of both aggregates. To describe these rotations we approximated the aggregates "A" and "B" by the structures which had opposite charges at the ends. In this case the observed rotational velocities of the aggregates "A" and "B" and the positions of rotation axes corresponded to charges at opposite ends of $+30$ and -50 e.u. for the aggregate "A" and $+90$ and -50 e.u. for the aggregate

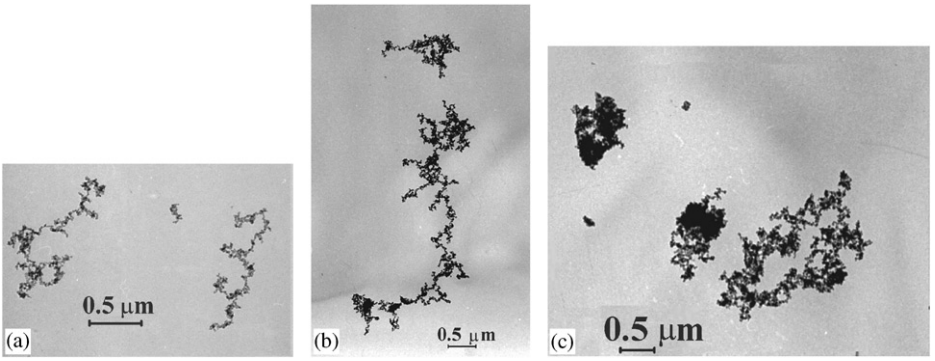

Fig. 20. TEM micrograms of soot aggregates formed at different times of coagulation t in the afterflame zone. (a) $t = 10$ s, chain-like aggregates; (b) $t = 140$ s, chain-like aggregates, and (c) $t = 1000$ s, compact aggregates. Initial time $t = 0$ s corresponds to the moment of sucking at the height above burner of 30 cm (see Fig. 1).

"B". Further, we switched off the electric field and observed the movement of these two aggregates in the absence of any external influences (Figs. 21a–e). The aggregates stuck to each other by ends which had the charges +90 and −50 (Fig. 21e). We also found that the aggregates approached each other with acceleration in the sticking process. The reason for this acceleration approach lies apparently in the Coulomb interactions between the aggregates. This assumption about the interactions is supported by the fact that the aggregates change the relative orientation in the sticking process (Figs. 21a–e). After the sticking we observe the restructuring of the newly formed aggregate. During this restructuring the oppositely charged ends stick to each other (Figs. 21e–h). This aggregate restructuring is similar to the restructuring of aggregates from chain-like structure to close-packed structure (Kops, Dibbets, Hermans, & Van de Vate, 1975; Schmidt-Ott, 1988, Weber et al., 1996; Jang & Friedlander, 1998; di Stasio, 2001b) that previous authors explained in terms of settlement of thermal energy. Thus, in our case the main factor in restructuring seems to be minimization of Coulomb energy.

4. Conclusions

Evolution of soot aggregate morphology, size and concentration is investigated during and after formation of soot in propane/air diffusion flame. It is determined that in flame the soot fractal dimension D_f is decreasing from 2.5 to 1.7 with the height above burner increasing from 2 to 11 cm. This decrease of D_f is explained by the decrease of the contribution of surface reactions to the growth of soot aggregates.

Measurements with an imaging system demonstrated that soot aggregates sampled from the flame are mostly charged. About 20% of aggregates sampled from the flame were neutral, 50% were positively charged and 30% were negatively charged. The ratios between the negative, positive and neutral aggregates do not depend on the sampling height above burner in the range 1.5–5 cm. The typical aggregate charge is about a few elementary units. Some aggregates are dipoles which is proved by aggregate revolutions when changing the polarity of the electric field applied.

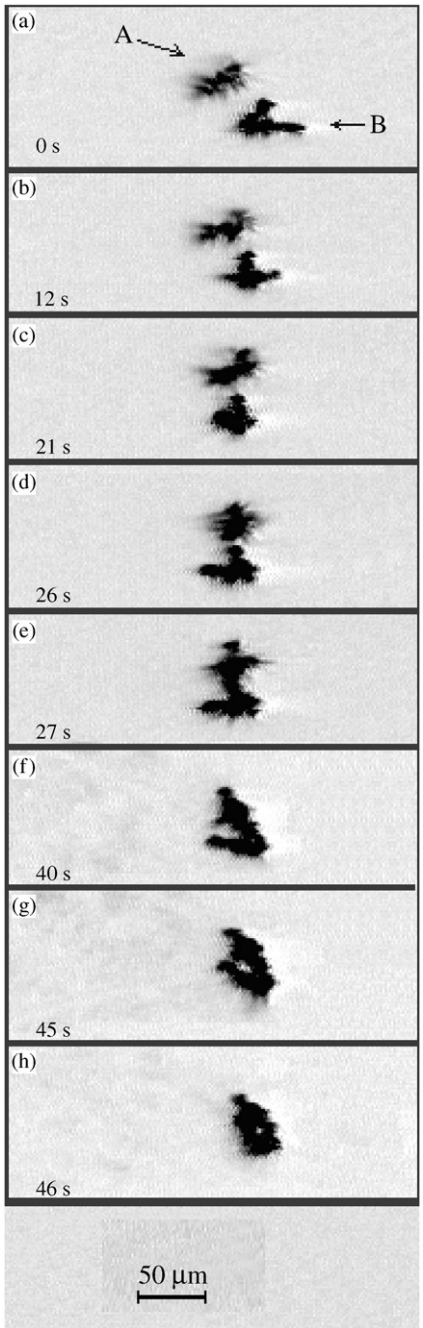

Fig. 21. A consequence of frames illustrating the mutual approach of two aggregates, sticking and restructuring of new formed aggregate.

It is determined that Coulomb interactions play an important role in soot deposition to the wall resulting in dendrite structure formation at the surface. This influence is demonstrated by an accelerated approach in aggregate–dendrite sticking process.

It is found that Coulomb interactions may affect considerably the aggregate–aggregate sticking process. This influence is demonstrated by changing the orientation and by accelerated mutual approach when sticking.

An effect of soot aggregate restructuring resulting in transformation of chain-like aggregates to compact structures was observed during the coagulation at room temperature. This effect is demonstrated directly by video observations. This restructuring is reflected also by simultaneous decrease of the aggregate radius from 0.4 to 0.15 μm and increase of D_f from 1.7 to 2.4 with coagulation time increasing in the range 200–1000 s. The observed aggregate transformation is explainable in terms of the Coulomb interactions between different parts of the aggregate.

Acknowledgements

This work was supported by the Russian Foundation for Basic Research (Project 01-03-32390) and by the Grant INTAS 2000-00460.

References

Ankilov, A., Baklanov, A., Mavliev, R., & Eremenko, S. (1991). Comparison of the Novosibirsk automated diffusion battery with the Vienna electro mobility spectrometer. *Journal of Aerosol Science*, *22*, S.325–S.328.

Appel, J., Bockhorn, H., & Frenklach, M. (2000). Kinetic modeling of soot formation with detailed chemistry and physics: Laminar premixed flames of C_2 hydrocarbons. *Combustion and Flame*, *121*, 122–136.

Ball, R. T., & Howard, J. B. (1971). Electric charge of carbon particle in flames. *Proceedings of the 13th International Symposium on Combustion*, Vol. 353, The Combustion Institute, Pittsburg.

Benish, T. G., Lafeur, A. L., Taghizadeh, K., & Howard, J. B. (1996). C_2H_2 and PAH as soot growth reactants in premixed C_2H_4-air flames. *Proceedings of the 26th Symposium (International) on Combustion*, The Combustion Institute, Pittsburg, pp. 2319–2326.

Bochhorn, H., & Schäfer, T. (1994). Growth of soot particles in premixed flames by surface reactions. In H. Bockhorn (Ed.), *Soot formation in combustion* (pp. 253–273). Berlin: Springer.

Calcote, H. F., & Gill, R. J. (1994). Comparison of the ionic mechanism of soot formation with a free radical mechanism. In H. Bockhorn (Ed.), *Soot formation in combustion* (pp. 471–482). Berlin: Springer.

D'Anna, A., D'Alessio, A., & Minutolo, P. (1994). Spectroscopic and chemical characterization of soot inception processes in premixed laminar flames at atmospheric pressure. In H. Bockhorn (Ed.), *Soot formation in combustion* (pp. 83–103). Berlin: Springer.

di Stasio, S. (2001a). Electron microscopy evidence of aggregation under three different size scales for soot nano-particles in flame. *Carbon*, *39*, 109–118.

di Stasio, S. (2001b). Observation of restructuring of nanoparticles of soot aggregates in a diffusion flame by static light scattering. *Journal of Aerosol Science*, *32*, 509–524.

Dobbins, R. A., & Subramaniasivan, H. (1994). Soot precursor particles in flames. In H. Bockhorn (Ed.), *Soot formation in combustion* (pp. 290–301). Berlin: Springer.

Forrest, S. R., & Witten Jr., T. A. (1979). Long-range correlations in smoke-particle aggregates. *Journal of Physics A: Mathematical and General*, *12*, L109–L117.

Frenklach, M., & Wang, H. (1994). Detailed mechanism and modeling of soot particle formation. In H. Bockhorn (Ed.), *Soot formation in combustion* (pp. 165–190). Berlin: Springer.

Fuchs, N. A. (1964). *The mechanics of aerosols*. Oxford: Pergamon Press.

Fuchs, N. A., & Petrianov, I. V. (1933). Measurement of size and charge of fog particles. *Journal of Physical Chemistry (Russia)*, *4*, 567–571.

Hurd, A. J., & Flower, W. L. (1988). In situ growth and structure of fractal silica aggregates in a flame. *Journal of Colloid and Interface Science*, *122*, 178–192.

Jang, H. D., & Friedlander, S. K. (1998). Restructuring of chain aggregates of titania nanoparticles in the gas phase. *Aerosol Science and Technology*, *29*, 81–91.

Julien, R., & Meakin, P. (1989). Simple models for the restructuring of three-dimensional ballistic aggregates. *Journal of Colloid and Interface science*, *127*, 265–272.

Kaskan, W. E. (1956). The dependence of flame temperature on mass burning velocity. *Proceedings of the Sixth Symposium (International) on Combustion* (pp. 134–143). New York: Reinhold.

Katzer, M., Weber, A. P., & Kasper, G. (2001a). The effects of electric fields on growth of titania particles formed in a CH_4-O_2 diffusion flame. *Journal of Aerosol Science*, *32*, 1045–1067.

Katzer, M., Weber, A. P., & Kasper, G. (2001b). Collision kinetics and electrostatic dispersion of airborne submicrometer fractal agglomerates. *Journal of Colloid and Interface Science*, *240*, 67–77.

Knorre, V. G., Tanke, D., Thienel, Th., & Wagner, H. Gr. (1996). Soot formation in the pyrolysis of benzene/acetylene and acetylene/hydrogen mixtures at high carbon concentrations. *Proceedings of the 26th Symposium (International) on Combustion*, The Combustion Institute, Pittsburg (pp. 2303–2310).

Kops, J., Dibbets, G., Hermans, L., & Van de Vate, J. F. (1975). The aerodynamic diameter of branched chain-like aggregates. *Journal of Aerosol Science*, *6*, 329–333.

Koshland, C. P. (1996). Impacts and control of air toxics from combustion. *Proceedings of the 26th Symposium (International) on Combustion*, The Combustion Institute, Pittsburg (pp. 2049–2065).

Köylü, Ü. O., Mcenally, C. S., Rosner, D. E., & Pfefferle, L. D. (1997). Simultaneous measurements of soot volume fraction and particle size/microstructure in flames using a thermophoretic sampling technique. *Combustion and Flame*, *110*, 494–507.

Longwell, J. P. (1982). The formation of polycyclic aromatic hydrocarbons by combustion. *Proceedings of the 19th Symposium (International) on Combustion*, The Combustion Institute, Pittsburg (pp. 1339–1350).

Macadam, S., Beer, J. M., Sarofim, A. F., & Hoffmann, A. B. (1996). Soot surface growth by polycyclic aromatic hydrocarbon and acetylene addition. *Proceedings of the 26th Symposium (International) on Combustion*, The Combustion Institute, Pittsburg (pp. 2295–2302).

Marquardt, M., Mauß, F., Jungfleisch, B., Suntz, R., & Bockhorn, H. (1996). Reinitiation of soot surface growth in premixed counter-flow flames. *Proceedings of the 26th Symposium (International) on Combustion*, The Combustion Institute, Pittsburg (pp. 2343–2350).

Martin, J. E., Schaefer, D. W., & Hurd, A. J. (1986). Fractal geometry of vapor phase aggregates. *Physical Review A*, *33*, 3540–3543.

Mauss, F., Trilken, B., Breitbachh, H., & Peters, N. (1994). Soot formation in partially premixed diffusion flames at atmospheric pressure. In H. Bockhorn (Ed.), *Soot formation in combustion* (pp. 325–349). Berlin: Springer.

Megaridis, C. M., & Dobbins, R. A. (1989). Comparison of soot growth and oxidation in smoking and non-smoking diffusion flames. *Combustion Science and Technology*, *66*, 1–16.

Nemeth, A., & Heberger, K. (1998). Computer modeling of formation of soot precursors in the oxidation of methane. *Berichte der Bunsen-Gesellschaft*, *102*, 257–261.

Onischuk, A. A., di Stasio, S., Karasev, V. V., Strunin, V. P., Baklanov, A. M., & Panfilov, V. N. (2000). Evidence for long-range Coulomb effects during formation of nanoparticle aggregates from pyrolysis and combustion routes. *Journal of Physical Chemistry A*, *104*, 10426–10434.

Place, E. R., & Weinberg, F. J. (1966). Electrical control of flame carbon. *Proceedings of the Royal Society A*, *289*(1417), 192–205.

Reilly, P. T. A., Gieray, R. A., Whitten, W. B., & Ramsey, J. M. (2000). Direct observation of the evolution of the soot carbonization process in the acetylene diffusion flame via real-time aerosol mass spectrometry. *Combustion and Flame*, *121*, 90–104.

Richter, R., Sander, L. M., & Cheng, Z. (1984). Computer simulations of soot aggregates. *Journal of Colloid and Interface Science*, *100*, 203–209.

Rogak, S. N., Baltensperger, U., & Flagan, R. C. (1991). Measurement of mass transfer to agglomerate aerosols. *Aerosol Science and Technology*, *14*, 447–458.

Rogak, S. N., Flagan, R. C., & Nguyen, H. V. (1993). The mobility and structure of aerosol agglomerates. *Aerosol Science and Technology*, *18*, 25–47.

Roth, P., & Hospital, A. (1994). Mass growth of charged soot particles in premixed flames. In H. Bockhorn (Ed.), *Soot formation in combustion* (pp. 239–251). Berlin: Springer.

Samson, R. J., Mulholland, G. W., & Gentry, J. W. (1987). Structural analysis of soot agglomerates. *Langmuir*, *3*, 272–281.

Schmidt-Ott, A. (1988). New approaches to *in situ* characterization of ultrafine agglomerates. *Journal of Aerosol Science*, *19*, 553–563.

Vander Wal, R. L. (1996). Soot precursor material: Visualization via simultaneous LIF-LII and characterization via TEM. *Proceedings of the 26th Symposium (International) on Combustion*, The Combustion Institute, Pittsburg (pp. 2269–2275).

Weber, A. P., Baltensperger, U., Gäggeler, H. W., & Schmidt-Ott, A. (1996). In situ characterization and structure modification of agglomerated aerosol particles. *Journal of Aerosol Science*, *27*, 915–929.

Wersborg, B. L., Howard, J. B., & Williams, G. C. (1973). Physical mechanisms in carbon formation in flames. *Proceedings of the 14th International Symposium on Combustion*, Vol. 929, The Combustion Institute, Pittsburg.

Wiltzius, P. (1987). Hydrodynamic behaviour of fractal aggregates. *Physical Review Letters*, *58*, 710–713.

Zhang, H. X., Sorensen, C. M., Ramer, E. R., Olivier, B. J., & Merklin, J. F. (1988). In situ optical structure factor measurements of an aggregating soot aerosol. *Langmuir*, *4*, 867–871.